Will Nonlinear Peculiar Velocity and Inhomogeneous Reionization Spoil 21 cm Cosmology from the Epoch of Reionization?

Paul R. Shapiro,[1,*] Yi Mao,[1,2,†] Ilian T. Iliev,[3] Garrelt Mellema,[4] Kanan K. Datta,[4] Kyungjin Ahn,[5] and Jun Koda[6]

[1]*Department of Astronomy and Texas Cosmology Center, University of Texas, Austin, Texas 78712, USA*

[2]*Institut Lagrange de Paris, Institut d'Astrophysique de Paris, CNRS, UPMC Université Paris 06, UMR7095, 98 bis, boulevard Arago, F-75014 Paris, France*

[3]*Department of Physics and Astronomy, Astronomy Centre, Pevensey II Building, University of Sussex, Falmer, Brighton BN1 9QH, United Kingdom*

[4]*Department of Astronomy and Oskar Klein Centre, AlbaNova, Stockholm University, SE-106 91 Stockholm, Sweden*

[5]*Department of Earth Sciences, Chosun University, Gwangju 501-759, Korea*

[6]*Centre for Astrophysics and Supercomputing, Swinburne University of Technology, Hawthorn, Victoria 3122, Australia*

(Received 12 November 2012; published 9 April 2013)

The 21 cm background from the epoch of reionization is a promising cosmological probe: line-of-sight velocity fluctuations distort redshift, so brightness fluctuations in Fourier space depend upon angle, which linear theory shows can separate cosmological from astrophysical information. Nonlinear fluctuations in ionization, density, and velocity change this, however. The validity and accuracy of the separation scheme are tested here for the first time, by detailed reionization simulations. The scheme works reasonably well early in reionization ($\lesssim 40\%$ ionized), but not late ($\gtrsim 80\%$ ionized).

DOI: 10.1103/PhysRevLett.110.151301 PACS numbers: 98.80.Es, 95.75.Pq, 98.58.Ge

Introduction.—Neutral hydrogen atoms in the intergalactic medium (IGM) at high redshift contribute a diffuse background of redshifted 21 cm-line radiation which encodes a wealth of information about physical conditions in the early Universe at $z > 6$, during and before the epoch of reionization (EOR). To derive cosmological information from this, however, we must be able to separate the dependence of the signal on the background cosmology (i.e., total matter density fluctuations) from that on the complex astrophysical processes that cause the thermal and ionization state of the intergalactic gas to fluctuate. The anisotropy introduced by the peculiar velocity of the gas, induced by structure formation, is the key to this separation.

According to linear perturbation theory, the three-dimensional power spectrum of the 21 cm brightness temperature fluctuations (hereafter, "21 cm power spectrum") can be expressed as a sum of terms which depend on different powers of the cosine, $\mu_{\mathbf{k}}$, of the angle between the line-of-sight (LOS) $\mathbf{n}$ and the wave vector of a given Fourier mode $\mathbf{k}$ [1]. Different terms represent contributions from different sources of fluctuations, including fluctuations in the total matter density, velocity, and hydrogen ionized fraction, and thereby, in principle, provide a means of separating the effects of cosmology and astrophysics. In particular, future measurements, it is proposed [1], can be used to fit this theoretical dependence of the power spectrum on $\mu_{\mathbf{k}}$ to extract the total matter density power spectrum-the cosmological jewel.

The success of this approach, however, depends upon the validity of the linear $\mu_{\mathbf{k}}$ decomposition. While fluctuations in the total matter density at high redshift are of linear amplitude on large scales, the nonlinearity of small-scale structure in density, velocity, and reionization patchiness can leave its imprint on the 21 cm signal, which might result in nonlinear distortion in the 3D 21 cm power spectrum and so spoil the linear $\mu_{\mathbf{k}}$ decomposition. In what follows, we will examine this question. We will assess the accuracy of this method for deriving cosmological information from the 21 cm background by using the results of a new large-scale N-body + radiative transfer simulation of cosmic reionization as mock data. Our simulation volume $(425\ \mathrm{Mpc}/h)^3$ [comparable to the low-frequency array (LOFAR) [2] survey volume] is large enough to make the sampling errors smaller than the systematic errors.

The 21 cm power spectrum anisotropy in redshift space.—The observed frequency reflects both the cosmological redshift $z_{\cos}$ from the time of emission and the Doppler shift associated with the peculiar radial velocity $v_{\parallel}$ there. In the "distorted" comoving coordinate system known as redshift space, the position of the emitter is the apparent comoving position if the redshift is interpreted as cosmological only, which shifts the real comoving coordinate $\mathbf{r}$ along the LOS to $\mathbf{s} = \mathbf{r} + \frac{1+z_{\cos}}{H(z_{\cos})} v_{\parallel}\mathbf{n}$ [where $H(z)$ is the Hubble parameter]. Henceforth, superscripts "r" and "s" denote quantities in real- and redshift space, respectively, and we will write z for $z_{\cos}$.

The 21 cm signal in redshift space can be modeled as follows, based on different assumptions on peculiar velocity and reionization patchiness.

(i) Linear scheme (linear velocity-density relation, linearized neutral fraction fluctuations): The linear scheme was originally proposed in the context of linear perturbation theory [1] and later rederived with weaker assumptions [3]

which are (1) the velocity ($\mathbf{v}^r$) and total density fluctuations (δ^r_ρ) satisfy the linear relation, $\widetilde{v^r_\parallel}(\mathbf{k}) = i(\frac{H(z)}{1+z})\widetilde{\delta^r_\rho}(\mathbf{k})\mu_\mathbf{k}/k$, (2) the baryon distribution traces the cold dark matter (CDM), (3) the peculiar velocity, the hydrogen density fluctuation ($\delta^r_{\rho_\mathrm{H}}$), and the neutral fraction fluctuation ($\delta^r_{x_\mathrm{HI}}$) are all linearized. Under these assumptions, the 3D 21 cm power spectrum can be expanded in polynomials of $\mu_\mathbf{k} \equiv \mathbf{k}\cdot\mathbf{n}/|\mathbf{k}|$,

$$P^{s,\mathrm{lin}}_{\Delta T}(\mathbf{k}, z) = P_{\mu^0}(k, z) + P_{\mu^2}(k, z)\mu^2_\mathbf{k} + P_{\mu^4}(k, z)\mu^4_\mathbf{k}. \quad (1)$$

While the 0th and 2nd moments are "contaminated" by power spectra due to reionization and/or spin temperature, the 4th moment depends only on $P^{r,\mathrm{total}}_{\delta_\rho,\delta_\rho}$ (total density power spectrum) and $\bar{x}_{\mathrm{HI},m}(z)$ (mass-weighted global neutral fraction),

$$P_{\mu^4}(k, z) = \widehat{\delta T}^2_b(z)P^{r,\mathrm{total}}_{\delta_\rho,\delta_\rho}(k, z), \quad (2)$$

where $\widehat{\delta T}_b$ is the mean 21 cm signal, $\widehat{\delta T}_b(z) = (23.88\ \mathrm{mK})(\frac{\Omega_b h^2}{0.02})\sqrt{\frac{0.15}{\Omega_\mathrm{M}h^2}\frac{1+z}{10}}\bar{x}_{\mathrm{HI},m}(z)$. Here, we focus on the limit where the spin temperature $T^r_s \gg T_\mathrm{CMB}$, valid soon after reionization begins. As such, we can neglect the dependence on spin temperature, but our discussion can be readily generalized to the case of finite T^r_s. In principle, then, cosmological information can be extracted from the 21 cm signal by fitting the measured $P^s_{\Delta T}(\mathbf{k}, z)$ to Eq. (1) to isolate the 4th moment.

(ii) Quasilinear $\mu_\mathbf{k}$-decomposition scheme (linear velocity-density relation, linearized neutral overdensity): The assumption of $\delta^r_{x_\mathrm{HI}} \ll 1$ breaks down when $\bar{x}_{\mathrm{HI},m} < 0.5$ [4]. Fortunately, Eqs. (1) and (2) can still hold, if we adopt the same assumptions (1) and (2) as in the linear scheme, but assume peculiar velocity and the neutral density fluctuation $\delta^r_{\rho_\mathrm{HI}} = \delta^r_{\rho_\mathrm{H}} + \delta^r_{x_\mathrm{HI}} + \delta^r_{\rho_\mathrm{H}}\delta^r_{x_\mathrm{HI}}$, as opposed to $\delta^r_{x_\mathrm{HI}}$ alone, are linearized. In this so-called quasilinear $\mu_\mathbf{k}$-decomposition formalism [3], only lower moments differ from the linear scheme prediction.

(iii) Fully nonlinear scheme (nonlinear velocity, nonlinear neutral overdensity): In the optically-thin approximation, two nonlinear effects of peculiar velocity must be taken into account: (1) the 21 cm brightness temperature is corrected for velocity gradient [1], $\delta T^s_b(\mathbf{s}) = \delta T^r_b(\mathbf{r}) = \widehat{\delta T}_b(z)\frac{1+\delta^r_{\rho_\mathrm{HI}}(\mathbf{r})}{|1+\delta^r_{\partial_r v}(\mathbf{r})|}$, where $\delta^r_{\partial_r v}(\mathbf{r}) \equiv \frac{1+z}{H(z)}\frac{dv_\parallel}{dr_\parallel}(\mathbf{r})$ is the gradient of proper radial peculiar velocity along the LOS, normalized by $\frac{H}{1+z}$; (2) when the real-space comoving coordinates $\mathbf{r}$ are mapped to redshift-space coordinates, volume elements are also resized according to $\delta V^s(\mathbf{s}) = \delta V^r(\mathbf{r})|1 + \delta^r_{\partial_r v}(\mathbf{r})|$. Fortunately, the combined effect allows us to compute the 21 cm brightness temperature in redshift space with a simple formula [3], $\delta T^s_b(\mathbf{s}) = \widehat{\delta T}_b(z)[1 + \delta^s_{\rho_\mathrm{HI}}(\mathbf{s})]$, where $\delta^s_{\rho_\mathrm{HI}}(\mathbf{s}) = n^s_\mathrm{HI}(\mathbf{s})/\bar{n}_\mathrm{HI}(z) - 1$ is the neutral overdensity in redshift space.

Angular separation of 3D power spectrum.—The moments of 3D power spectrum can be decomposed using the χ^2 fit as follows. For a given LOS, 3D modes $P^s_{\Delta T}(\mathbf{k})$ with the same $\mu_\mathbf{k}$ and same k but different azimuthal angle are averaged to give a measure of $\overline{P^s_{\Delta T}}(k, \mu_\mathbf{k})$ and the associated sampling variance $\sigma^2_P(k, \mu_\mathbf{k}) = (2/N_{\mu_\mathbf{k},k})\overline{P^s_{\Delta T}}^2(k, \mu_\mathbf{k})$, where $N_{\mu_\mathbf{k},k}$ is the number of modes with the same $\mu_\mathbf{k}$ and k. For the 3D grid from the simulated data, we further combine the measures along three different LOS, tripling the number of modes. Next, modes are grouped in spherical k shells with the width $\Delta k/k = 0.186$ (chosen as a trade-off between minimal mean χ^2 and minimal numerical noise, but our results below are insensitive to this value). For each shell (the k dependence is implicit below), we shall fit the data set $\{\mu_i, \overline{P^s_{\Delta T}}(\mu_i), \sigma_P(\mu_i)\}$ (where i runs through all modes within the shell) with the ansatz $P^s_{\Delta T}(\mu) = \sum_{j=1}^3 a_j X_j(\mu)$, where basis functions $X_j(\mu) = \{1, \mu^2, \mu^4\}$ and coefficients $a_j = \{P_{\mu^0}, P_{\mu^2}, P_{\mu^4}\}$, for $j = 1, 2, 3$, respectively. We employ the standard general linear least squares method (see, e.g., Ref. [5]) for the χ^2 fit. This results in best-fit coefficients $a_j = \sum_{k=1}^3 C_{jk}\beta_k$ with associated error estimates $\sigma(a_j) = \sqrt{C_{jj}}$. Here, we define the 3×3 matrix $\alpha_{jk} = \sum_i X_j(\mu_i)X_k(\mu_i)/\sigma^2_P(\mu_i)$, whose inverse is the covariance matrix $C = \alpha^{-1}$, and a 3-vector $\beta_j = \sum_i \overline{P^s_{\Delta T}}(\mu_i)X_j(\mu_i)/\sigma^2_P(\mu_i)$.

Mock data from a reionization simulation.—We perform a new large-scale, high-resolution N-body simulation of the ΛCDM universe (performed with the CubeP^{3}M code [6,7]) in a comoving volume of 425 Mpc/h on each side using 5488^3 (165 billion) particles. To find halos, we use the spherical overdensity method and require them to consist of at least 20 N-body particles; this implies a minimum halo mass of $10^9 M_\odot$. We use subgrid modeling to compute the halo population with mass between 10^8–$10^9 M_\odot$. Assuming that the gas traces the CDM particles exactly, we grid the density and velocity in the IGM (i.e., halo mass excluded) on a 504^3 grid using SPH-like smoothing with an adaptive kernel. Halo lists and density fields are then processed with the radiative transfer code C^{2}Ray [8]. Each halo releases f_γ ionizing photons per baryon per $\Delta t = 11.5$ Myrs, with $f_\gamma = 8.2$ ($f_\gamma = 2$) for halos below $10^9 M_\odot$ (above $10^9 M_\odot$), respectively. To incorporate feedback from reionization, halos less massive than $10^9 M_\odot$ located in ionized regions do not produce any photons. We refer the readers to Ref. [9] and Iliev *et al.* [10] for more details of this simulation. The background cosmology is consistent with the WMAP Collaboration seven-year results [11]: $\Omega_\Lambda = 0.73$, $\Omega_M = 0.27$, $\Omega_b = 0.044$, $h = 0.7$, $\sigma_8 = 0.8$, $n_s = 0.96$.

We then calculate the nonlinear 3D 21 cm power spectrum, using the mesh-to-mesh real-to-redshift-space-mapping (MM-RRM) scheme in Ref. [3] for mapping the nonlinear density, velocity, and ionization grid data from the simulation in real space onto a redshift space grid, and separate out the best-fit 4th moment using the aforementioned angular separation prescription. The linear and quasilinear schemes both predict that this 4th moment should be given by Eq. (2), which we test by evaluating the rhs of Eq. (2) directly from the simulation N-body results, for comparison. Some preliminary results were previously summarized by us in Ref. [12].

Results and discussions.—In Fig. 1, we plot the best-fit 4th moment of the fully nonlinear power spectrum and the benchmark linear expectation. Note that, while the mock 21 cm signal is from the IGM, as is the observed signal, the total density power spectrum is expected in the linear scheme. (There is a difference between the total and IGM density power spectra, as in Fig. 1, resulting from the exclusion of particle mass in halos when computing the IGM density.) We focus on the range of wave numbers, $0.2 < k < 1h$ Mpc^{-1}, for which k is large enough to avoid a large sampling variance but small enough to avoid a large aliasing effect.

(i) Consistency check of the decomposition pipeline: We confirm that: (1) the total density power spectrum from N-body simulation agrees with the linear power spectrum (from CAMB [13]) at large scales $k \lesssim 0.5h$ Mpc^{-1}. At smaller scales, it agrees with the result from the third-order perturbation theory (3PT) [14], but is enhanced relative to the linear power spectrum. (2) The best-fit 4th moment agrees with the total density power spectrum at $z = 30$ when the IGM is everywhere neutral and the density fluctuations are of linear amplitude.

(ii) Effect of IGM nonlinear density and velocity fluctuations: For diagnostic purposes, we first investigate the case in which the ionized fraction at each point in the IGM is set equal to the mass-weighted global ionization fraction $\bar{x}_{i,m}$ in the reionization simulation at that redshift. In this case, the best-fit 4th moment at different redshifts is enhanced with respect to the total density power spectrum, and the deviation increases from 20% ($z \simeq 14$) to 70% ($z \simeq 7$), as structure formation proceeds. These results show that nonlinear density and velocity fluctuations cause the $\mu_{\mathbf{k}}$ decomposition to make a systematic error, not caused by ionization patchiness.

(iii) Effect of inhomogeneous reionization and velocity fluctuations: Early in reionization, the best-fit 4th moment for inhomogeneous reionization is suppressed relative to that for the homogeneously partially-ionized case. This is because fluctuations in neutral fraction and

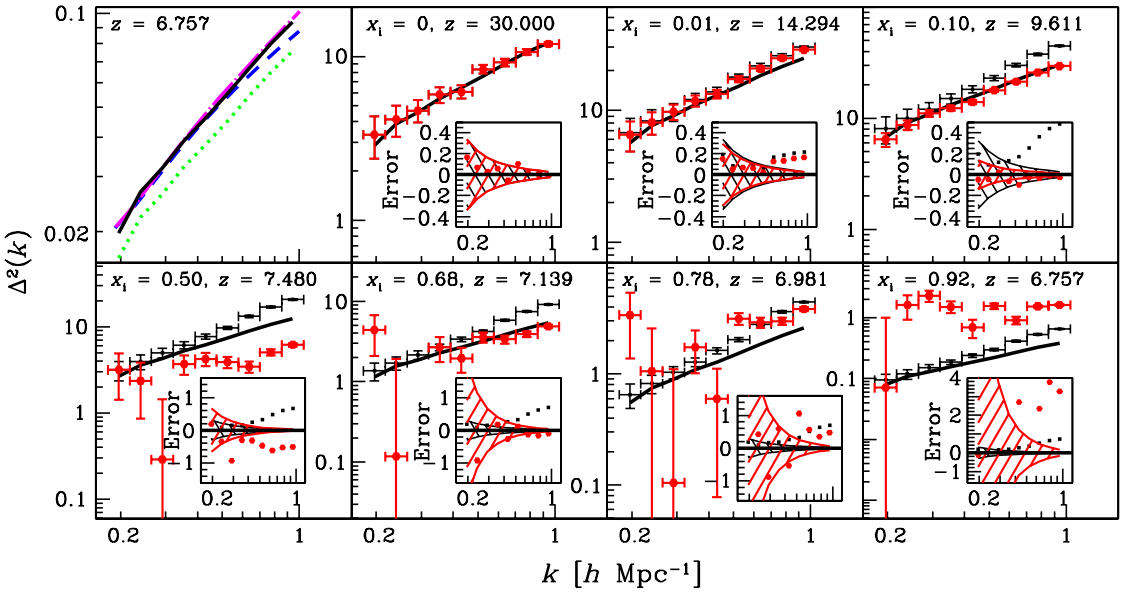

FIG. 1 (color online). Top left panel: the matter density power spectrum, $\Delta^2_{\delta\delta} = k^3 P_{\delta\delta}(k)/2\pi^2$ (unitless), from N-body results for total matter (solid or black) and for IGM matter (green or dot), linear total density (dashed or blue), and 3PT total density (dot-dashed or magenta), at $z = 6.757$. Other panels: the total matter density power spectrum [multiplied by $\widehat{\delta T_b}^2(z)$] as "measured" by fitting the mock data (i.e., reionization simulation) for the 3D 21 cm power spectrum to the $\mu_{\mathbf{k}}$ decomposition, $\Delta^2_{\mu^4} = k^3 P_{\mu^4}(k)/2\pi^2$ (in mK^2), at different phases of reionization ($\bar{x}_{i,m} = 0$, 0.01, 0.10, 0.50, 0.68, 0.78, and 0.92, respectively). Red data points are reionization simulation results. Black data points assume homogeneously ionized IGM with same $\bar{x}_{i,m}$ as reionization simulation. Solid black curves are the expectation from linear scheme, $P^{\rm linear}_{\mu^4}$, i.e., Eq. (2) evaluated using total density power spectra from N-body simulation [multiplied by $\widehat{\delta T_b}^2(z)$]. Plotted in inset are fractional systematic errors, i.e., $(P^{\rm best-fit}_{\mu^4} - P^{\rm linear}_{\mu^4})/P^{\rm linear}_{\mu^4}$. We also plot the sampling errors (due to the simulation volume) for the best-fit 4th moment, $\sigma(P_{\mu^4})$, as error bars, and the fractional sampling errors, $\sigma(P_{\mu^4})/P^{\rm linear}_{\mu^4}$, as shaded regions in inset.

density anticorrelate in a universe reionized "inside out"; i.e., overdense regions are ionized earlier on average than underdense regions. This anticorrelation affects the anisotropy of the 21 cm power spectrum through the coupling of nonlinear ionization fluctuations with velocity fluctuations (which are, themselves, correlated with density fluctuations). Otherwise, reionization patchiness, alone, cannot introduce anisotropy in the 21 cm power spectrum (e.g., as in the quasilinear $\mu_{\mathbf{k}}$ decomposition scheme). A more quantitative explanation will be formulated in detail in Mao *et al.* [15].

This effect cancels the enhancement due to nonlinear fluctuations in IGM density and velocity, alone. Incidentally, the fractional systematic error first crosses zero (less than 10% at all scales) when $\bar{x}_{i,m} \approx 10\%$ ($z \simeq 9.6$ in our simulation). Afterwards, this error grows to 60% for $\bar{x}_{i,m} \lesssim 50\%$. As determined by the competition between these two effects, this error depends on both the reionization epoch and the scale of interest — the smaller the ionized fraction $\bar{x}_{i,m}$ and the smaller the wave number k, the smaller the error (see Fig. 2).

As the typical size of ionized regions grows larger than the scales plotted here, the best-fit 4th moment at $k = 0.5$–$1h$ Mpc^{-1} becomes less suppressed after the 50% ionized epoch. For this k-range, the net error changes sign again when $\bar{x}_{i,m} \simeq 68\%$ (with error $<20\%$).

At late epochs ($\bar{x}_{i,m} \gtrsim 0.8$, $z \lesssim 7$), the fractional systematic error for all scales is large, $\gtrsim 100\%$. This is due to the breakdown of the perturbative expansion, i.e., the expansion of the 3D 21 cm power spectrum in neutral density fluctuations becomes divergent when $\delta_{\rho_{\rm HI}} \gtrsim \mathcal{O}(1)$, as the ionized bubbles expand and percolate in the Universe. In addition, while our calculation does not include the light cone effect [16], this effect becomes non-negligible at this late time and can further squeeze the anisotropic power spectrum along the LOS, as does the redshift space distortion. Therefore, the estimate of 100% error here is only a lower limit to the actual error at late times.

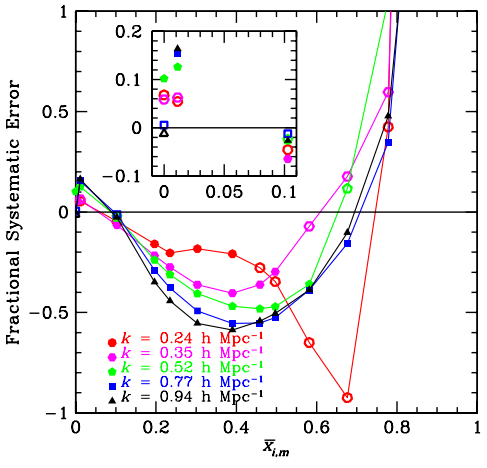

FIG. 2 (color online). The fractional systematic error of the separation scheme, in the inhomogeneous reionization case, as a function of $\bar{x}_{i,m}$, for $k = 0.24$, 0.35, 0.52, 0.77, $0.94h$ Mpc^{-1}, respectively. The solid (open) dots correspond to the case where the systematic error is greater (less) than the sampling error of our simulation. The inset is a zoom-in to $0 \leq \bar{x}_{i,m} \leq 0.10$.

(iv) The sampling variance: Our simulation volume is large enough that these systematic errors quoted above are all greater than the estimated sampling errors (except when the systematic error crosses zero), so they represent statistically significant deviations from the expectations of the $\mu_{\mathbf{k}}$ decomposition, rather than accidents of the particular numerical realization.

In the homogeneously ionized case (denoted by the superscript "H" below), the fractional sampling error for the 4th moment, $\sigma(P_{\mu^4})/P^{\rm linear}_{\mu^4}$, remains constant over time, which is a consequence of the unchanging number of modes. However, the fractional sampling error evolves dramatically during inhomogeneous reionization (denoted by the superscript "I"), for reasons as follows. For each ring with given values of $\mu_{\mathbf{k}}$ and k, sampling errors of power spectra satisfy $\sigma_P^I/\sigma_P^H = \overline{P^{s,I}_{\Delta T}}/\overline{P^{s,H}_{\Delta T}} \equiv \eta(k, \mu_{\mathbf{k}})$, since $N_{\mu_{\mathbf{k}},k}$ is the same for both cases. If, for simplicity, η is only a function of k, then it is straightforward to show that $\frac{\sigma^I(P_{\mu^4})/P^{\rm linear}_{\mu^4}}{\sigma^H(P_{\mu^4})/P^{\rm linear}_{\mu^4}} = \eta$. Over time η evolves from less than to greater than unity, because (1) in the early phase of reionization, the density power spectrum is dominant, but the $\delta^r_{\rho_{\rm H}}$-$\delta^r_{x_{\rm HI}}$ anticorrelation decreases the total power, and (2) in the late phase, the ionization power dominates over the density power spectrum.

Conclusion.—This Letter is the first attempt to quantify, in detail, the intrinsic precision of the linear scheme for extracting the cosmological matter density power spectrum from 21 cm observations of the EOR. [A recent paper [17] considered the Legendre decomposition of the anisotropic 21 cm power spectrum, using seminumerical simulations, but only showed the results for monopole and quadrupole, not hexadecapole (4th-moment equivalent), due to large error bars in their simulations.] Two effects may spoil the extraction, a major one due to the coupling between inhomogeneous reionization and velocity fluctuations and a minor one due to nonlinear density and velocity fluctuations alone. The competition between these identifies two phases of reionization particularly interesting to cosmology—$\bar{x}_{i,m} \simeq 68\%$, where fractional systematic error is within 20% for $k = 0.5$–$1h$ Mpc^{-1}, and $\bar{x}_{i,m} \simeq 10\%$, where this error is within 10% for all wave numbers. The epoch of exact crossover is likely to depend on the reionization scenario.

We summarize our results in Fig. 2. We see that, for the early phase of reionization $\bar{x}_{i,m} < 40\%$, the linear $\mu_{\mathbf{k}}$ decomposition works well for large-scale measurement $k \lesssim 0.24h$ Mpc^{-1}, with errors within 20%. At smaller

scales, down to $k \simeq 0.5h$ Mpc^{-1}, errors are within 50%. During the intermediate phase ($\bar{x}_{i,m} \simeq 0.4$–0.7), using the $\mu_{\mathbf{k}}$ decomposition at the intermediate k range 0.35–$0.5h$ Mpc^{-1} can also result in errors within 50%. However, in the late phase ($\bar{x}_{i,m} \gtrsim 0.8$), it is difficult to extract the cosmological information from 21 cm observations using the $\mu_{\mathbf{k}}$ decomposition, unless possibly at very large scales $k < 0.2h$ Mpc^{-1}.

This work was supported in part by NSF Grants No. AST-0708176 and No. AST-1009799, NASA Grants No. NNX07AH09G, No. NNG04G177G, and No. NNX11AE09G, Chandra Grant No. SAO TM8-9009X, the French state funds managed by the ANR within the Investissements d'Avenir programme under Reference No. ANR-11-IDEX-0004-02, the Science and Technology Facilities Council [Grants No. ST/F002858/1 and No. ST/I000976/1], the Southeast Physics Network (SEPNet), the Swedish Research Council Grant No. 2009-4088, and the National Research Foundation of Korea (NRF) grant funded by the Ministry of Education, Science and Technology (MEST; Grants No. 2012M4A2026720 and 2012R1A1A1014646). The authors acknowledge the Texas Advanced Computing Center (TACC) and the National Institute for Computational Sciences (NICS) for providing HPC resources, under NSF TeraGrid Grants No. TG-AST0900005 and No. TG-080028N and TACC internal allocation Grant No. "A-asoz." Computations were performed on the GPC supercomputer at the SciNet HPC Consortium. SciNet is funded by: the Canada Foundation for Innovation under the auspices of Compute Canada, the Government of Ontario, Ontario Research Fund-Research Excellence, and the University of Toronto.

*shapiro@astro.as.utexas.edu
†mao@iap.fr

[1] R. Barkana and A. Loeb, Astrophys. J. Lett. **624**, L65 (2005).
[2] M. P. van Haarlem *et al.* (to be published), http://www.lofar.org.
[3] Y. Mao, P. R. Shapiro, G. Mellema, I. T. Iliev, J. Koda, and K. Ahn, Mon. Not. R. Astron. Soc. **422**, 926 (2012).
[4] A. Lidz, O. Zahn, M. McQuinn, M. Zaldarriaga, and S. Dutta, Astrophys. J. **659**, 865 (2007).
[5] W. H. Press, S. A. Teukolsky, W. T. Vetterling, and B. P. Flannery, *Numerical Recipes: The Art of Scientific Computing* (Cambridge University Press, Cambridge, 2007), 3rd ed., p. 665.
[6] I. T. Iliev, P. R. Shapiro, G. Mellema, H. Merz, and U.-L. Pen, arXiv:0806.2887.
[7] J. Harnois-Deraps, U.-L. Pen, I. T. Iliev, H. Merz, J. D. Emberson, and V. Desjacques, arXiv:1208.5098.
[8] G. Mellema, I. T. Iliev, M. A. Alvarez, and P. R. Shapiro, New Astron. **11**, 374 (2006).
[9] I. T. Iliev, G. Mellema, P. R. Shapiro, U.-L. Pen, Y. Mao, J. Koda, and K. Ahn, Mon. Not. R. Astron. Soc. **423**, 2222 (2012).
[10] I. T. Iliev *et al.* (to be published).
[11] E. Komatsu *et al.* (WMAP Collaboration), Astrophys. J. Suppl. Ser. **192**, 18 (2011).
[12] Y. Mao, P. R. Shapiro, I. T. Iliev, G. Mellema, J. Koda, and U.-L. Pen, Astron. Soc. Pac. Conf. Ser. **432**, 212 (2010).
[13] A. Lewis and S. Bridle, Phys. Rev. D **66**, 103511 (2002); see also http://camb.info/.
[14] D. Jeong and E. Komatsu, Astrophys. J. **651**, 619 (2006).
[15] Y. Mao *et al.* (to be published).
[16] K. K. Datta, G. Mellema, Y. Mao, I. T. Iliev, P. R. Shapiro, and K. Ahn, Mon. Not. R. Astron. Soc. **424**, 1877 (2012).
[17] S. Majumdar, S. Bharadwaj, and T. R. Choudhury, arXiv:1209.4762.